Design and implementation of droop control in *d-q* frame for islanded microgrids

Estefanía Planas*, Asier-Gil-de-Muro**, Jon Andreu*, Iñigo Kortabarria*, Iñigo Martínez de Alegría* *University of the Basque Country UPV/EHU, 48013, Bilbao, Spain, e-mail: *estefania.planas@ehu.es* **TECNALIA, Energy Unit. Parque Tecnologico de Bizkaia, 48160, Derio, Spain, e-mail: *asier.gildemuro@tecnalia.com*

Abstract

Droop control method is usually used when distributed energy sources are connected in parallel. The absence of communications between the distributed energy resources and its flexibility are some of its advantages. Moreover, a fictitious impedance can be added which improves the performance of the original technique. This fictitious impedance has to be properly designed in order to obtain a good stability and performance of the system. On the other hand, a restoration control that brings frequency and voltage amplitude of the microgrid to their nominal values is used in some cases. In this article, a lineal model of a droop controlled microgrid with fictitious impedance and restoration control is implemented. Thanks to this lineal model, an optimal fictitious impedance can be designed. Moreover, the influence of a proposed restoration control on the whole system can be studied. This way, the dynamic of the restoration control can be properly chosen. The stability as well as nominal values of frequency and voltage amplitude are guaranteed. Experimental results of the system confirm the validity of the proposed design.

I. Introduction

Renewable energy sources are presented by most governments as principal candidates to cover the future demand reducing environmental impact in comparison with traditional energy sources such as carbon, fuel, etc. The reason is majorly due to the global concerns over the amount of greenhouse gases (GHGs) emitted to the atmosphere when these fuels are burnt

[1]. In this sense, electric microgrids are a good option for integrating different types of distributed generation systems, exploiting the available resources in each place (wind, sun, biomass, etc.). A microgrid can be defined as a group of distributed generators, distributed storages and variety of customer loads [2]. A microgrid is able to operate with only a small power exchange with the rest of the system and can be connected or disconnected from the main grid. A microgrid differs from existing island power systems (both physical islands and electrical islands, such as offshore oil/gas platforms, ships and aircraft) in that connection to and disconnection from a public grid is a regular event [3].

These small grids, formed by several distributed generators and loads, are characterised by their high efficiency, good quality power supply and the reduction of environmentally unfriendly emissions [4]–[7] In these microgrids, several power converters can operate as voltage sources in order to enhance the stability in island behaviour. The stability of these microgrids has been addressed in several works by developing state-space models of microgrids [8], [9] and small-signal stability studies [10], [11]. On the other hand, voltage differences may appear when several power voltage sources are connected in parallel because of tolerances mismatches, line impedances, etc. These voltage differences can cause circulating currents between the voltage sources [12]. These currents have to be controlled since they can be harmful for the equipments, specially in cases of low load. Many control methods have been proposed in order to avoid those circulating currents and to guarantee a good performance of the system [13]. In case of microgrids, frequency-droop and voltage-droop control strategies are often used to share real and reactive power components [5], [14].

The droop methods are based on the inductive behaviour of the impedances between the coupled power converters and the grid [15]. Thanks to this inductive behaviour, decoupling of active and reactive powers is obtained and they can be controlled separately [16]. This impedance is influenced by the output impedance of the power converters and the line characteristics, so the inductive behaviour is not guaranteed in all cases. Coupling inductances are sometimes used to guarantee an inductive behaviour, however they increment the size, cost and weight of the system [17]. One proposed approach to guarantee an inductive behaviour of the output impedance is to add a fictitious impedance in the control loop [18]. Many

publications have developed this concept [13], [19]–[23] obtaining other advantages in terms of stability, dynamic response, etc. However, this fictitious impedance has to be carefully designed since it affects the stability of the whole system. In [13] a transfer function that characterizes the output impedance of uninterruptible power systems (UPS) is used to design this fictitious impedance. In [24] small-signal models using complex number matrix are used to design properly the fictitious impedance.

In this work, a lineal model of a microgrid in *d-q* frame is implemented. This model consists on several transfer functions that relates the circulating current, voltage and frequency of one experimental microgrid with the load and frequency and voltage offsets of the control of the microgrid. Thanks to this model, the behaviour of the circulating current for different fictitious impedances can be analysed. Therefore, a suitable value for the fictitious impedance that guarantees the stability of the system and minimizes the circulating current can be found.

On the other hand, droop methods have an inherent trade-off between the power sharing and the voltage and frequency regulation. Adaptive droops have been proposed in order to minimize the deviation of the voltage and frequency of the droop-controlled microgrids in [25], [26]. Some other work eliminate these deviations by a restoration control based on integrators [27], [28]. This work proposes a control that is also based on integrators, but with a dynamic specified in each power converter. Thanks to this, the dynamic of the restoration control can be adapted to each power converter in order to guarantee the stability of the system. In addition, low bandwith communications can be employed since the restoration signals are stationary values. The selection of the dynamic of the restoration control is also carried out by means of the implemented lineal model of the microgrid. Finally, experimental results that validate the proposed design are provided.

II. Droop control for microgrids

A. Fundamentals of the droop method

The droop method is based on the performance of synchronous generators where the impedance between them and the grid is often considered inductive [5], [19]. There are two main reasons for this consideration. The first is the inductive behaviour of the output

impedance of these generators and the second is that they are usually connected to high-voltage lines which behaviour is mainly inductive. Thanks to this, decoupling between active and reactive powers is obtained and they can be controlled separately. In [29] it is proposed to reproduce this behaviour artificially in power converters adding the following expressions to each converter:

$$\omega_{droop,i}{}^{*} = \omega_{nom} - m_i \cdot (P_i - P_{nom,i}), \tag{1}$$

$$V_{droop,i}{}^{*} = V_{nom} - n_i \cdot (Q_i - Q_{nom,i}), \tag{2}$$

where *i* represents each converter, ω_{nom} and V_{nom} are the nominal frequency and amplitude of the system, P_i and Q_i are the actual active and reactive powers, and $P_{nom,i}$ and $Q_{nom,i}$ are the active and reactive powers of each power converter at nominal frequency and voltage. If these equations are represented in *d-q* frame, the frequency droop is maintained and the voltage droop equations can be chosen as follows [30]:

$$V_{droop,i,d}{}^{*} = V_{nom,d} - n_i \cdot (Q_i - Q_{nom,i}), \tag{3}$$

$$V_{droop,i,q}{}^{*} = 0V. \tag{4}$$

When non-controllable sources are used, such as renewable sources, some offsets can be added to (3), (4). These offsets are then calculated in order to balance the primary source power and the output power of the non-controllable source.

B. Fictitious impedance

The output impedance of power converters relies on, mainly, the internal impedance of the power converters and the line impedance. In [31] the emulation of a fictitious impedance inside the droop control method is proposed. This fictitious impedance has an inductive behaviour for the main frequency direct sequence and a resistive behaviour for the high frequency and unbalanced components. This way, besides the active and reactive power sharing, unbalanced components and harmonics sharing is also guaranteed. Other fictitious impedances can be

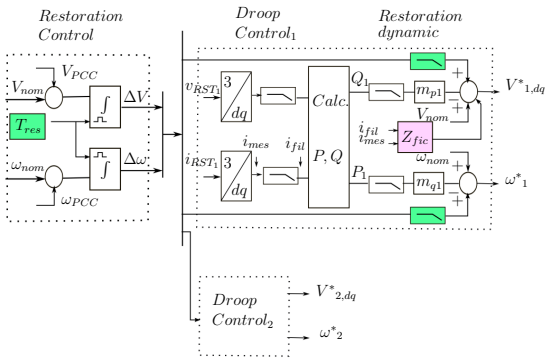

Fig. 1. Control scheme of the droop method with fictitious impedance and the restoration control.

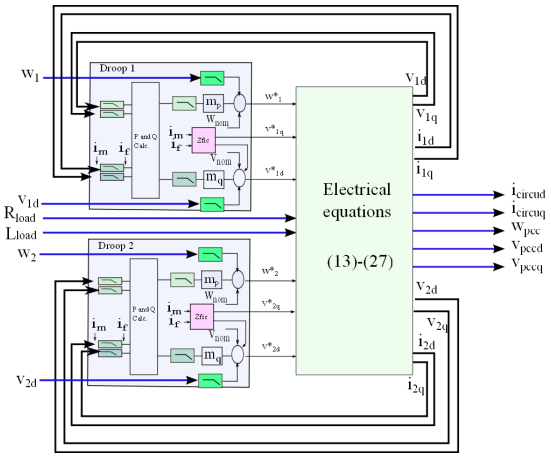

Fig. 2. Scheme of the whole system which is linealized.

found in [17], [21], [22]. In [30], a *d-q* frame is adopted to implement a fictitious impedance being the voltage droop across this:

$$V_{i,fic,d} = -i_{i,fil,d} \cdot X_{i,fic} + (i_{i,mes,d} - i_{i,fil,d}) \cdot R_{i,fic}, \tag{5}$$

$$V_{i,fic,q} = i_{i,fil,q} \cdot X_{i,fic} + (i_{i,mes,q} - i_{i,fil,q}) \cdot R_{i,fic}, \tag{6}$$

where $V_{i,fic,d}$ and $V_{i,fic,q}$ represent the voltage droop in the fictitious impedance, $R_{i,fic}$ and $X_{i,fic}$ the values of the fictitious resistance and inductor respectively, and $i_{i,fil,dq}$ and $i_{i,mes,dq}$ are the values of the filtered and non filtered currents of each power converter respectively.

It has to be noticed that there is no need to calculate each component since the same resistive impedance value for the unbalanced currents and the harmonic components is used,.

This way, the solution is much easier to implement from the computational point of view. In the same manner, the resistance component helps soften the current oscillations when jumps of load, frequency, etc. appears. The values of $R_{i,fic}$ and $X_{i,fic}$ has to be carefully chosen in order to improve the behaviour of the system. If the selected values are not suitable, a worse behaviour or even an unstable performance can be obtained. In the present work, a lineal model of the whole system is implemented that considers both the electrical part and the control part of the microgrid. Thanks to this model, the values of the fictitious impedance can be properly chosen. This model is presented in section III.

C. Restoration control

The inherent trade-off between power sharing and voltage regulation is one drawback of the droop method. A restoration control based on integrators is proposed in some works [27], [28]. These restoration controls correct the deviations of frequency and voltage amplitude from their nominal values. It has to be noticed, that if an integrator is placed in each power converter, restoration set-points for each power converter may be different. These differences can be caused by measurement mismatches and different initial conditions on the integrators. Therefore, this restoration control has to be carried out in a centralized way. Some form of communication is needed to send the corresponding references from the central restoration controller to the power converters. It is desirable to have non-critical and low-bandwidth communications for getting a robust system. In this work, a central controller that sends the restoration references to the power converters has been implemented. This control is also based on integrators, but the dynamic is specified in each power converter. Thanks to this, a proper dynamic can be chosen in each converter in order to maintain the stability of the whole system. The following equations describe the restoration control:

$$V_{i,rest,d} = \int (v_{pcc,d} - v_{nom,d})dt \cdot \frac{\omega_{rest,i,c}}{s + \omega_{rest,i,c}}, \tag{7}$$

$$V_{i,rest,q} = 0V, \tag{8}$$

$$\omega_{i,rest} = \int (\omega_{pcc} - \omega_{nom})dt \cdot \frac{\omega_{rest,i,c}}{s + \omega_{rest,i,c}}, \tag{9}$$

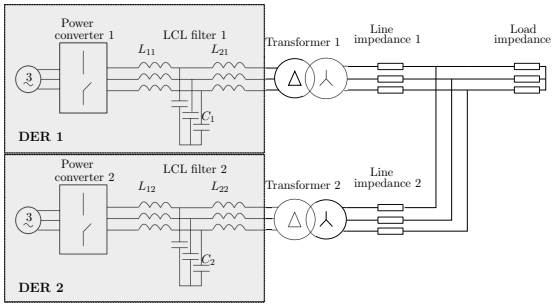

Fig. 3. Electrical scheme of the studied microgrid.

where v_{pcc} and ω_{pcc} are the measured voltage and frequency in the point of common coupling (PCC) by the central controller respectively, v_{nom} and ω_{nom} are the nominal voltage amplitude and frequency respectively, and $\omega_{rest,i,c}$ is the dynamic of the restoration control. The v_{pcc} corresponds to v_{pcc1} in fig. 4 and the central controller defines the sample time of the integrator (T_{rest} in fig. 1).

It is important to notice that low-bandwidth communications can be used for the central controller since the restoration signals, the output of the integrals in (7),(9) are stationary values. The parameter $\omega_{rest,i,c}$ defines the dynamic of the restoration control and the associated low pass filter is placed in each power converter. This way the dynamic of the restoration control is defined in each power converter and can be designed taking into account different inercias of the DERs. The whole control scheme is shown in fig. 1. Taking into account (1)-(9), the final equations that describe the control are:

$$\omega_i^* = {\omega_{droop,i}}^* + \omega_{i,rest}, \tag{10}$$

$$V_{i,d}^* = {V_{droop,i,d}}^* - V_{i,fic,d} + V_{i,rest,d}, \tag{11}$$

$$V_{i,q}^* = -V_{fic,q}. \tag{12}$$

The restoration dynamic also affects the stability and performance of the system. Therefore, a suitable dynamic has to be designed. In this manner, the same lineal model implemented in this work is used to chose a proper dynamic of the restoration control. The lineal model and the droop control design is explained on the following section.

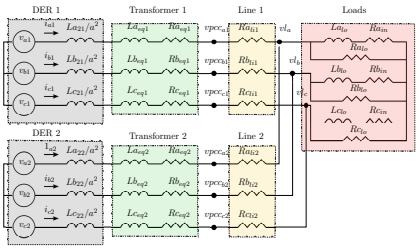

Fig. 4. Equivalent circuit of the analysed microgrid.

TABLE I
PARAMETERS OF THE EQUIVALENT CIRCUIT.

DER, Load		**Transformer**		**Line**	
$\lvert v_{a,b,c}\rvert$	220 Vrms	a	$(\sqrt{3}\cdot 251)/400$	$R_{li,1}$	0.1 Ω
R_{load}	34.8 Ω	$R_{eq,1,2}$	0.05 Ω	$L_{li,1,2}$	0.1 mH
L_{load}	123.2 mH	$L_{eq1,2}$	0.09 mH	$R_{li,2}$	0.2 Ω
R_{in}	3.8 Ω				
$L_{a,b,c,ii}$	0.6 mH				

III. LINEAL MODEL OF A MICROGRID

A. Model of the electrical scheme

A three-phase AC experimental microgrid formed by two three-phase DER (Distributed Energy Resource) and feeding several RL loads has been studied (fig. 3). An equivalent circuit of this electric scheme is presented in fig. 4. In this scheme, DER units are modelled as controllable and independent voltage sources. This is acceptable since the flexibility of control of power converters is high and the voltage on the output filter of the DERs is totally controllable. The equivalent circuit of the transformer can be described as the series equivalent impedance and the magnetizing branch. Only the series impedance has been considered since the current across the magnetizing branch is insignificant comparing with the current in the series branch. The inductances $L_{abc,ij}$ corresponds to the second inductance of the LCL filter but referred to the secondary of the transformer. With the aim of referring this inductance to the secondary, its value is divided into the square of the turns ratio (L/a^2). The values of the equivalent circuit are shown in table I. The currents and voltages of the voltage source 1 on fig. 4 are described in the *d-q* frame as follows:

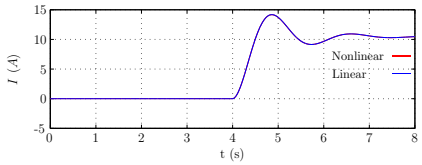

(a) Component d of the circulating current.

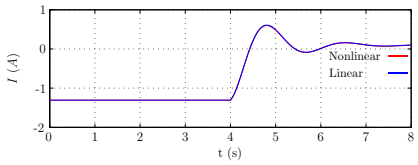

(b) Component q of the circulating current.

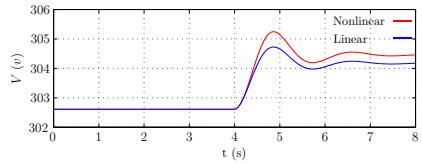

(c) Component d of the voltage on the PCC.

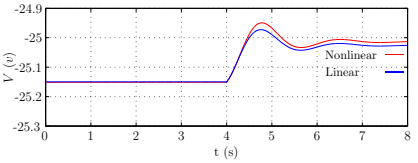

(d) Component q of the voltage on the PCC.

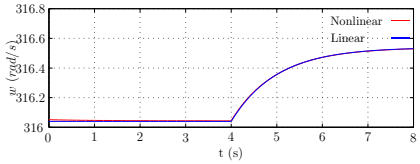

(e) Frequency of the voltage on the PCC.

Fig. 5. Responses of the lineal and nonlineal system to a step perturbation in the frequency offset.

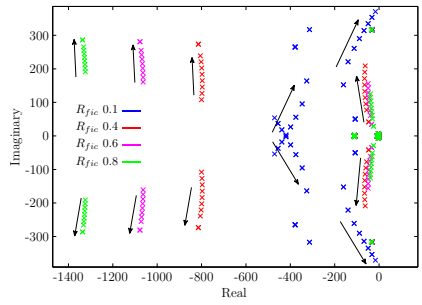

(a) Map of poles.

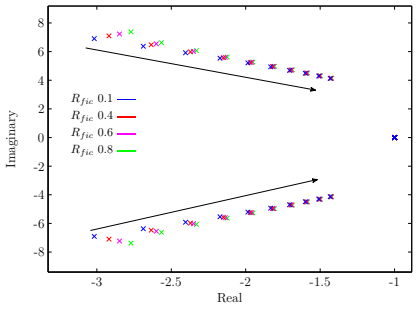

(b) Zoom of the map of poles.

Fig. 6. Map of poles of the obtained transfer functions for different values of R_{fic} and X_{fic}.

$$\frac{di_{i,d}}{dt} = \frac{-R_{eqi}}{L_{2i}+L_{eqi}} \cdot i_{di} + \frac{1}{L_{2i}+L_{eqi}} \cdot (v_{i,d} - v_{pcci,d}), \quad (13)$$
$$+\omega_{sc} \cdot i_{i,q}$$

$$\frac{di_{i,q}}{dt} = \frac{-R_{eqi}}{L_{2i}+L_{eqi}} \cdot i_{qi} + \frac{1}{L_{2i}+L_{eqi}} \cdot (v_{i,d} - v_{pcci,d}), \quad (14)$$
$$-\omega_{sc} \cdot i_{i,d}$$

$$\frac{dv_{pcci,d}}{dt} = A_1 \cdot i_{i,d} - A_2 \cdot i_{i',d} - A_3 \cdot v_{pcci,d} \quad (15)$$
$$-A_4 \cdot v_{pcci',d} + A_5 \cdot v_{i,d} + A_4 \cdot v_{i',d} + \omega_{sc} \cdot v_{pcci,q},$$

$$\frac{dv_{pcci,q}}{dt} = A_1 \cdot i_{i,q} - A_2 \cdot i_{i',q} - A_3 \cdot v_{pcci,q} \quad (16)$$
$$-A_4 \cdot v_{pcci',q} + A_5 \cdot v_{i,q} + A_4 \cdot v_{i',q} - \omega_{sc} \cdot v_{pcci,d},$$

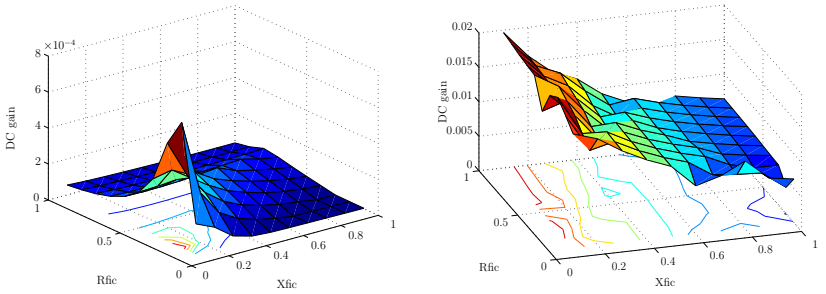

(a) DC gain of the transfer function $i_{circ,d}/R_{load}$.

(b) DC gain of the transfer function $i_{circ,q}/R_{load}$.

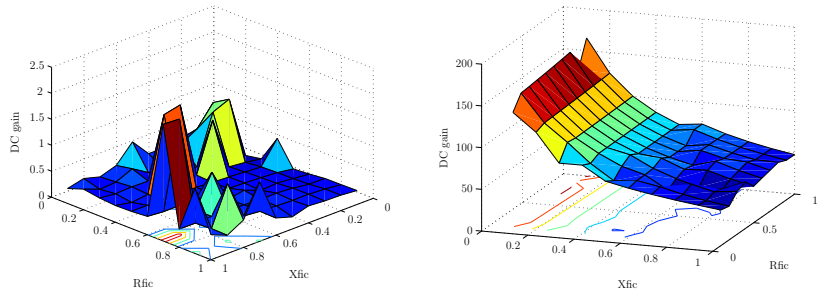

(c) DC gain of the transfer function $i_{circ,d}/L_{load}$.

(d) DC gain of the transfer function $i_{circ,q}/L_{load}$.

Fig. 7. DC gain of the *d-q* circulating current for different values of R_{fic} and L_{fic}.

TABLE II
Droop CHARACTERISTICS.

Control parameters			
$m_{p1,2}$	$1.57 \cdot 10^{-4}$	$R_{fic1,2}$	0.6 Ω
$m_{q1,2}$	$9.11 \cdot 10^{-5}$	$X_{fic1,2}$	0.8 Ω
$V_{nom,d}$	220 Vrms	$Q_{nom1,2}$	40 kVA
$P_{nom1,2}$	50 kW	n	10
$\omega_{pot,c}$	1 rad/s	$\omega_{mes,c}$	100 $\cdot 2\pi$ rad/s
$\omega_{rest,c1,2}$	1 rad/s	T_{rest}	2 s

where

$$A_1 = \frac{R_{lii} \cdot (R_{lo} + R_{in}) + R_{lo} \cdot R_{in}}{L_{lo}} - \frac{R_{eqi} \cdot (R_{lii} + R_{lo}}{L_{2i} + L_{eqi}},$$
$$A_2 = \frac{R_{eqi'} \cdot R_{lo}}{L_{2i'} + L_{eqi'}} + \frac{R_{lo} \cdot R_{in}}{L_{lo}}), A_4 = \frac{R_{lo}}{L_{2i'} + L_{eqi'}},$$
$$A_3 = \frac{R_{lii} + R_{lo}}{L_{2i} + L_{eqi}} + \frac{R_{lo} + R_{in}}{L_{lo}}, A_5 = \frac{R_{lii} + R_{lo}}{L_{2i} + L_{eqi}},$$

and *i* refers to one power converter and *i'* to the other one. In these equations, there are some terms that rely on the frequency of the *d-q* frame.

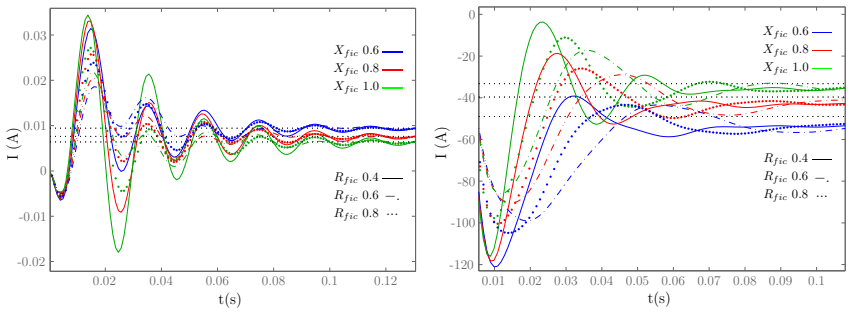

(a) Step response of $i_{circ,q}/R_{load}$.

(b) Step response of $i_{circ,q}/L_{load}$.

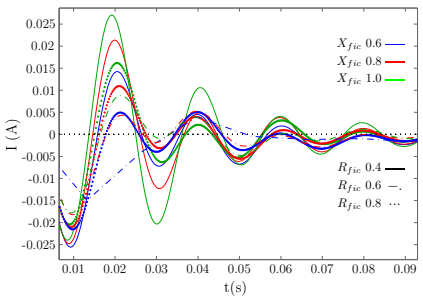

(c) Step response of $i_{circ,d}/R_{load}$.

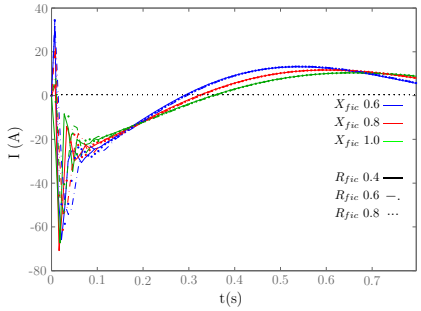

(d) Step response of $i_{circ,d}/L_{load}$.

Fig. 8. Step response of the circulating current for different values of R_{fic} and X_{fic}.

These equations refer to unique *d-q* frame, as each system has its own frequency and *d-q* frame, the output voltage values must be transformed to a unique *d-q* frame. For the present case with two power converters, the references provided by the droop control of each converter are adapted to a common reference frame as follows:

$$\theta/2 = \frac{1}{2}\int(\omega_1 - \omega_2), \tag{17}$$

$$v_{1,d,sc} = v_{1,d} \cdot cos(\theta/2) - v_{1,q} \cdot sin(\theta/2), \tag{18}$$

$$v_{1,q,sc} = v_{1,q} \cdot cos(\theta/2) + v_{1,d} \cdot sin(\theta/2), \tag{19}$$

$$v_{2,d,sc} = v_{2,d} \cdot cos(\theta/2) + v_{1,q} \cdot sin(\theta/2), \tag{20}$$

$$v_{2,q,sc} = v_{2,q} \cdot cos(\theta/2) - v_{2,d} \cdot sin(\theta/2), \tag{21}$$

$$w_{sc} = (\omega_1 + \omega_2)/2. \tag{22}$$

Considering small deviations of frequency between the power converters (*cos(θ) ≈ 1 and sin(θ) ≈ θ*), (18)-(21) are:

$$v_{1,d,sc} = v_{1,d} - v_{1,q} \cdot \theta/2, \tag{23}$$

$$v_{1,q,sc} = v_{1,q} + v_{1,d} \cdot \theta/2, \tag{24}$$

$$v_{2,d,sc} = v_{2,d} + v_{1,q} \cdot \theta/2, \tag{25}$$

$$v_{2,q,sc} = v_{2,q} - v_{2,d} \cdot \theta/2, \tag{26}$$

An important variable to measure the stability of the system is the circulating current between the power converters. This current is:

$$i_{circ,dq} = \frac{i_{1,dq} - i_{2,dq}}{2}. \tag{27}$$

On the other hand, it has to be considered that (13)-(16) and (23)-(26) are non lineal equation since they present products between several variables. In the same manner, R_{load} and L_{load} terms appear as constants in (13)-(16) but normally load jumps are expected in microgrids. If they are considered as variables, the performance of the circulating current for different load values can be studied for designing the fictitious impedance. By linearising these equations around an operation point, transfer functions that describe the performance of the system can be obtained.

B. Model of the droop control

The model of the droop control is presented in (1)-(10) and it is observed that it is described by lineal equations. On the other hand, products between currents and voltages are necessary to calculate active and reactive powers. These products are non lineal terms and must be also be linearised.

C. Lineal model of the whole system

The system in fig. 2 has been built by means of Matlab-Simulink R2008a software in a simulink model. A block-by-block analytic linearization has been implemented that linearizes the blocks individually and then combines the results to produce the linearization of the whole

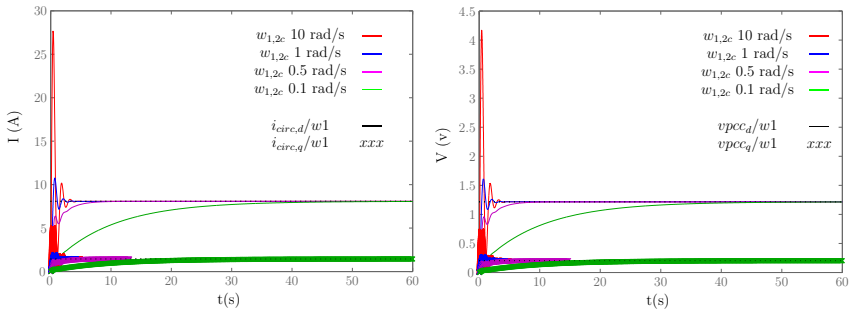

(a) Step response of $i_{circ,d}/w1$ and $i_{circ,q}/w1$.

(b) Step response of $vpcc_d/w1$ and $vpcc_q/w1$.

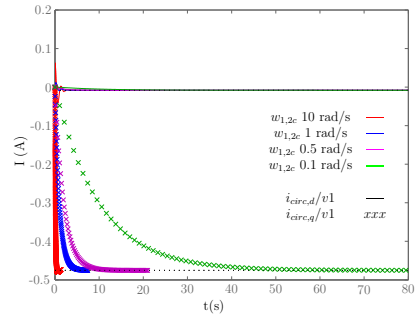

(c) Step response of $i_{circ,d}/v1$ and $i_{circ,q}/v1$.

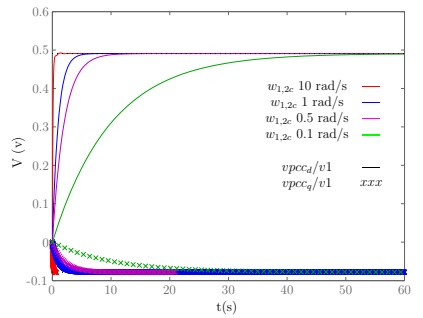

(d) Step response of $vpcc_d/v1$ and $vpcc_q/v1$.

Fig. 9. Step response of the circulating current and voltage on the PCC to changes in the frequency offset of the restoration control

system. This method has several advantages as support of open-loop analysis, control of the linearization of each block, etc.

Operation points for voltages, currents and frequency have to be selected in order to linearise the system around this operation point. Nominal values of frequency and voltages have been chosen as the operating points. For choosing the values of the load, it has been considered that the circulating current increases in cases of low load values. This way, a low value of active and reactive load have been chosen. The chosen operating points for the whole model are shown in tables I and II. The values of R_{load} and L_{load} correspond to a power of 1.39 kW and 1.25 kV, which is considered a low value of load taking into account the nominal value of the powers of the DER units (table II).

The original nonlinear system and the obtained linear systems have been compared adding a perturbation to both systems. In fig. 5 the responses of the lineal and non-lineal systems are shown for a perturbation in the frequency input ω_1 (fig. 2). Taking into account the behaviour it is concluded that the obtained lineal model is a good approximation of the non-lineal model.

IV. Design of the droop method

The nominal values of the frequency, voltage, active and reactive powers are chosen taking into account the specified specifications. The selected slopes relies on the desired tolerance of the frequency and voltage of the microgrid and are defined as follows:

$$m_i = \frac{2 \cdot \omega_{nom} \cdot tol_\omega}{P_{max} - P_{min}}, \tag{28}$$

$$n_i = \frac{2 \cdot v_{nom} \cdot tol_v}{Q_{max} - Q_{min}}, \tag{29}$$

where tol_ω and tol_v are the desired frequency and voltage tolerances respectively.

The droop method needs voltage and current measurements (1)-(4). The currents are measured and transformed by Clarke transform in order to isolate homopolar components. Then, the Park transform is used in order to obtain only the direct sequence. The rest of components appear with a frequency at least twice the value of the frequency of the Park transform. Active and reactive powers must be also calculated (1)-(4). These powers have to be filtered for eliminating possible noise and perturbations. The cut-off frequency of the filters define the inercia of each power converter as they would be traditional generators. A first order filter that improves the dynamic response of the power measurement has been used [30]:

$$F(s) = \frac{1 + \frac{s}{n \cdot \omega_{pot,c}}}{1 + \frac{s}{\omega_{pot,c}}} \tag{30}$$

where $\omega_{pot,c}$ is the cut-off frequency of the filter and *n* is a parameter that approaches the behaviour of this filter to a first order filter as it increases. The chosen values are presented in table II.

A. Design of a fictitious impedance

Transfer functions that describe the whole system have been obtained by the linearisation of the whole system. This way, transfer functions that relates each of these inputs (ω_1, v_1, R_{load}, L_{load}, ω_2, v_2, fig. 2) with each of these outputs ($i_{circu,d}$, $i_{circu,q}$, ω_{pcc},$v_{pcc,d}$, $v_{pcc,q}$, fig. 2) have been obtained. It has to be commented that all the obtained transfer functions share the same

poles. Thanks to this, the stability of the whole system can be analysed by the map of poles of any of the obtained transfer funtion. In the same manner, these transfer functions have different values for different fictitious impedances. It has to be considered that the voltage droop in the fictitious impedance increases with its value, so it is convenient to decrease it as much as possible. Therefore, the transfer functions obtained for fictitious impedances from 0.1 Ω till 1.0 Ω have been studied.

1) Stability of the system: first, the map of poles of these transfer functions for different fictitious impedances are shown in figs. 6(a) and 6(b). The closest poles to the origin does not practically move with the fictitious impedance (fig. 6(b)). However, in fig. 6(a), it is observed that the next poles get further from the real and imaginary axis as the X_{fic} increases for values of R_{fic} higher that 0.4 Ω, improving the stability of the system. In fig. 6(a) it is also shown how the following poles also gets further from the origin as the R_{fic} increases. So the next range of values is chosen in terms of stability: $R_{fic} > 0.4\ \Omega$ and $X_{fic} > 0.5\ \Omega$.

2) Minimization of the circulating current: secondly, the DC gain of the transfer functions $i_{circ,d}/R_{load}$ and $i_{circ,q}/R_{load}$ for different values of fictitious impedance has been studied (figs. 7(a)-7(d)). It is observed that the DC gain of $i_{circ,d}/R_{load}$ and $i_{circ,d}/L_{load}$ are slightly affected in comparison with $i_{circ,q}/R_{load}$ and $i_{circ,q}/L_{load}$. From values of X_{fic} higher of 0.6 Ω the DC gain comes much lower. In this manner, the selected range of values in order to minimize the circulating current is $X_{fic} > 0.6\ \Omega$.

3) Dynamic response of the system: thirdly, the step responses have been also studied in order to compare the dynamic performance for several values of fictitious impedance. It is observed that the peaks get smaller as the R_{fic} increases (figs. 8(a)-8(d)), but the responses become slower. So there is a trade-off between the transient response and the speed of the response. Taking into account all this, the selected range is $X_{fic} < 0.8\ \Omega$.

Considering the selected ranges of values for the fictitious impedance, a fictitious impedance of X_{fic} 0.8 Ω and R_{fic} 0.6 Ω has been chosen. In the map of poles (figs. 6(a), 6(b)) it is shown that the stability is similar to that obtained with a lower fictitious impedance. The DC gain of the studied transfer functions is also considered (figs. 7(a)-7(d)) and it is shown that a low value of DC gain is obtained with these values of fictitious impedance. The third factor

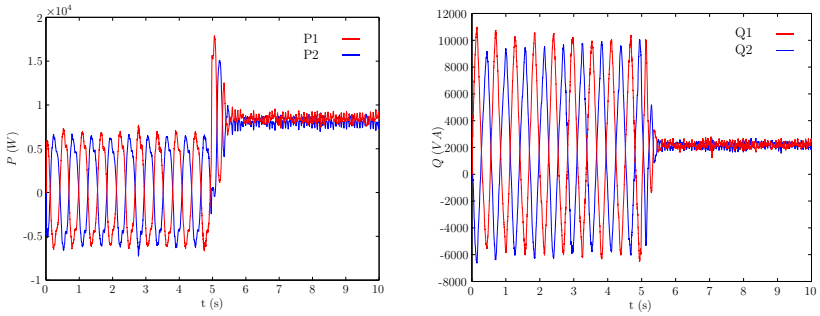

(a) Active power of DER1 and DER2 with a fictitious impedance of R_{fic} 0.1 Ω and X_{fic} 0.28 Ω.

(b) Reactive power of DER1 and DER2 with a fictitious impedance of R_{fic} 0.1 Ω and X_{fic} 0.28 Ω.

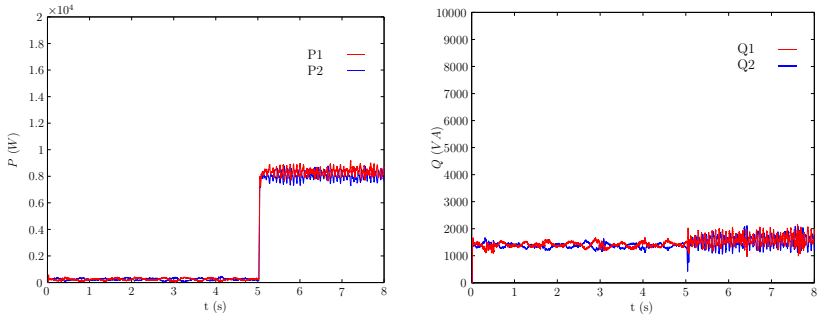

(c) Active power of DER1 and DER2 with a fictitious impedance of R_{fic} 0.6 Ω and X_{fic} 0.8 Ω.

(d) Reactive power of DER1 and DER2 with a fictitious impedance of R_{fic} 0.6 Ω and X_{fic} 0.8 Ω.

Fig. 10. Experimental results of the active and reactive powers of both DERs.

taken into account is the step response of the systems, specially (figs. 8(b) and 8(d)) where the dynamic response is more critical since the permanent values are more than 1000 times higher than the permanent values in (figs. 8(a) and 8(c)).

B. Design of restoration control

On the other hand, it is convenient to design properly the dynamic of the restoration control with the aim of maintaining the stability of the system. As this dynamic depends mainly of the selected $\omega_{rest,c}$ (7)-(9), the transfer functions that characterizes the behaviour to jumps in the restoration control signals of the voltage on the PCC ($v_{pcc,d}/\Delta\omega$, $v_{pcc,q}/\Delta\omega$, $v_{pcc,d}/\Delta V$ and $v_{pcc,q}/\Delta V$) and the circulating current ($i_{circ,d}/\Delta\omega$, $i_{circ,q}/\Delta\omega$, $i_{circ,d}/\Delta V$ and $i_{circ,q}/\Delta V$) and have been studied in order to choose a proper ω_c. The step responses for different $\omega_{rest,c}$ are shown in figs. 9(a)−9(d). It is shown that the dynamic response of the four transfer functions improves greatly as ω_c increases but the system becomes greatly slower. In the same manner, the system is more sensitive to changes in frequency, so the dynamic of $v_{pcc,d}/\Delta\omega$ and

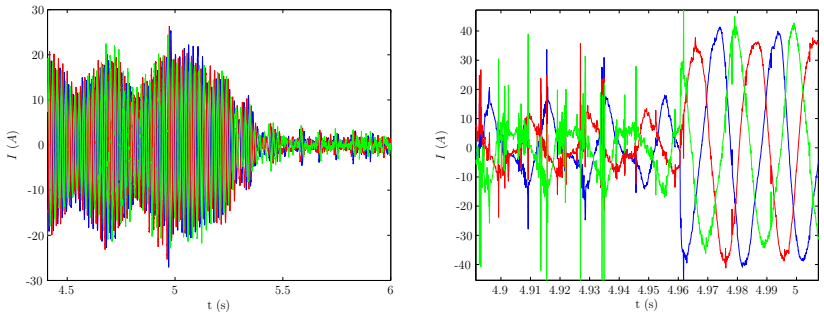

(a) Circulating current with a fictitious impedance of R_{fic} 0.1 Ω and X_{fic} 0.28 Ω.

(b) Load current with a fictitious impedance of R_{fic} 0.1 Ω and X_{fic} 0.28 Ω.

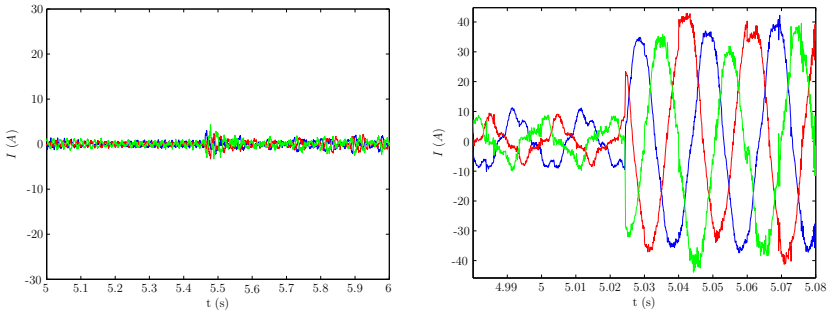

(c) Circulating current with a fictitious impedance of R_{fic} 0.6 Ω and X_{fic} 0.8 Ω.

(d) Load current with a fictitious impedance of R_{fic} 0.6 Ω and X_{fic} 0.8 Ω.

Fig. 11. Experimental results of both DERs with a fictitious impedance of R_{fic} 0.6 Ω and X_{fic} 0.8 Ω.

$v_{pcc,q}/\Delta\omega$ is specially considered. Therefore, there is also a trade-off between the speed and the transitory response of the system. In this case, an ω_c of 1 rad/s has been chosen since it guarantees a smooth transient response in a suitable time of response.

V. Experimental Results

The circuit presented in fig. 3 has been built. The characteristics of the built system are the same as the ones considered in the lineal model (tables I and II). In the experimental system, no additional impedance has been connected considering the inherent line impedance of the lines that connect the DERs with the loads. The values of the line impedance in the lineal model have been estimated in order to match with the ones in the experimental system. These experimental results has been obtained by a High Speed Data Adquisition Unit that stores data in a specified file. This file can be readen by a PC in order to graphic the results.

Initially, the system without the fictitious impedance has been tested, obtaining a very unstable system that made the protections of power converters to disconnect them from the

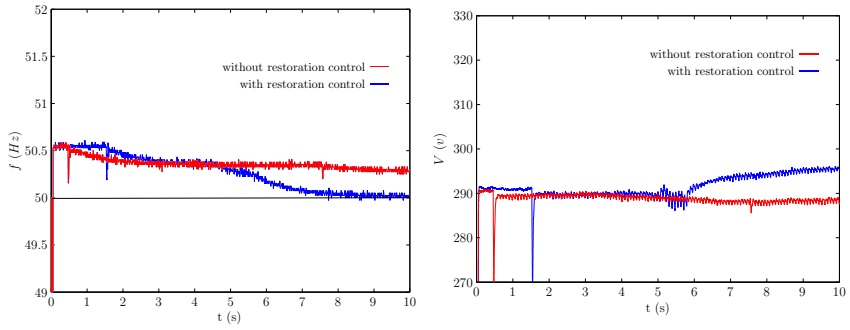

(a) Frequency in PCC.

(b) Voltage amplitude in PCC.

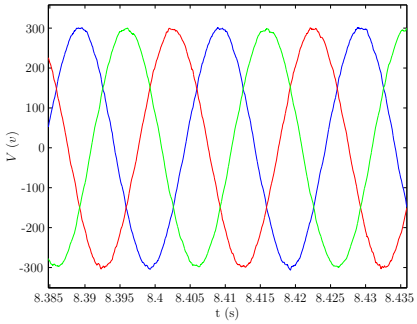

(c) Three-phase voltage in the PCC with the designed virtual impedance and restoration control.

Fig. 12. Experimental results of both DERs with a fictitious impedance of R_{fic} 0.6 Ω and X_{fic} 0.8 Ω and the restoration control.

circuit. Then, an initial value of fictitious impedance has been tested (R_{fic} 0.1 Ω and X_{fic} 0.28 Ω). The results obtained for no load shows that the circulating current gets very high values, placing the equipments in risk (figs. 10(a)-11(b)). Then a load of 16.6 kW and 1.25 kVA is connected and the system becomes more stable. It has to be mentioned that if the system continues without load, the protections of the DER units make them to disconnect from the grid. It has to be noticed that the measured reactive power does not match with the load value (Q=1.25 kVA). This increase is due to the reactive power consumed by the transformers (see fig. 3).

Then the chosen values for the fictitious impedance have been then tested. In figs. 10(c)-10(d) the active and reactive powers generated by both DER units are shown. It is observed that both DER units generate the same active and reactive power. It is also shown that the circulating current between the units is strongly lower in comparison with the one obtained with the first fictitious impedance (fig. 11(c)). The load current also improves (fig. 11(d)) and

the no load currents of the transformer are clearly shown.

The restoration control has been also tested. The results for the system with the designed fictitious impedance and with and without the restoration control are shown in figs. 12(a)-12(b). This way, it is observed that both the frequency and the voltage amplitude on the PCC are restored to their nominal values. Moreover, the restoration is smooth so that the nominal values are recovered without transitory oscillations. Taking into account all the experimental results, it can be concluded that the designed fictitious impedance improves the stability of the system and reduces the circulating current between the DERs. In addition, the voltage quality of the microgrid also has improved thanks to the implemented restoration control.

VI. Conclusions

Droop method has been used to control several power converters forming a microgrid. A fictitious impedance has been added in order to minimize the circulating current between the power converters. Moreover, a restoration control in *d-q* frame and with a dynamic specified in each power converter has been designed. The fictitious impedance values as well as the dynamic of the restoration control have been designed by means of a lineal model in *d-q* frame of the microgrid. In this model, electric scheme and the droop control with the fictitious impedance and the restoration control have been included. Thanks to this model, the droop method has been properly designed and the circulating current has been minimized. Moreover, the amplitude and the frequency of the voltage on the microgrid has been improved by means of the restoration control. Experimental results have been provided, they confirm the validity of the proposed system.

Acknowledgements

This work has been carried out inside de Research and Education Unit UFI11/16 of the UPV/EHU and supported by the Department of Education, Universities and Research of the Basque Government within the fund for research groups of the Basque university system IT394-10 and by the University of the Basque Country.

REFERENCES

[1] M. Akorede, H. Hizam, and E. Pouresmaeil, "Distributed energy resources and benefits to the environment," *Renewable and Sustainable Energy Reviews*, vol. 14, no. 2, pp. 724–734, 2010.

[2] N. Lidula and A. Rajapakse, "Microgrids research: A review of experimental microgrids and test systems," *Renewable and Sustainable Energy Reviews*, vol. 15, no. 1, pp. 186–202, 2011.

[3] T. Green and M. Prodanovic, "Control of inverter-based micro-grids," *Electric Power Systems Research*, vol. 77, no. 9, pp. 1204–1213, 2007.

[4] R. Rietz and S. Suryanarayanan, "A review of the application of analytic hierarchy process to the planning and operation of electric power microgrids," *North American Power Symposium (NAPS)*, pp. 1–6, 2008.

[5] F. Katiraei, R. Iravani, N. Hatziargyriou, and A. Dimeas, "Microgrids management," *IEEE Power and Energy Magazine*, vol. 9, pp. 54–65, 2011.

[6] A. Kumar, S. P. Chowdury, and S. Paul, "Microgrids: Energy management by strategic deployment of ders. a comprehensive survey," *Renewable and Sustainable Energy Reviews*, vol. 15, no. 9, pp. 4348–4356, 2011.

[7] N. Hatziargyriou, D. A., and A. Tsikalakis, "Centralized and decentralized control of microgrids," *International Journal of Distributed Energy Resources*, vol. 1, pp. 197–202, 2005.

[8] N. Pogaku, M. Prodanovic, and T. Green, "Modeling, analysis and testing of autonomous operation of an inverter-based microgrid," *IEEE Transactions on Power Electronics*, vol. 22, no. 2, pp. 613–625, 2007.

[9] H. Avelar, W. Parreira, J. Vieira, L. de Freitas, and E. Coelho, "A state equation model of a single-phase grid-connected inverter using a droop control scheme with extra phase shift control action," *IEEE Transactions on Industrial Electronics*, vol. 59, no. 3, pp. 1527–1537, 2012.

[10] Z. Zeng, H. Yang, and R. Zhao, "Study on small signal stability of microgrids: A review and a new approach," *Renewable and Sustainable Energy Reviews*, vol. 15, pp. 4818–4828, 2011.

[11] F. Katiraei, M. Iravani, and P. Lehn, "Small-signal dynamic model of a micro-grid including conventional and electronically interfaced distributed resources," *IET Generation, Transmission and Distribution*, vol. 1, no. 3, pp. 369–378, 2007.

[12] H. Cai, R. Zhao, and H. Yang, "Study on ideal operation status of parallel inverters," *IEEE Transactions on Power Electronics*, vol. 23, no. 6, pp. 2964–2969, 2008.

[13] J. Guerrero, L. Garcia de Vicuna, J. Matas, M. Castilla, and J. Miret, "Output impedance design of parallel-connected ups inverters with wireless load-sharing control," *IEEE Transactions of Industrial Electronics*, vol. 52, no. 4, pp. 1126–1135, 2005.

[14] R. Majumder, A. Ghosh, G. Ledwich, and F. Zare, "Load sharing and power quality enhanced operation of a distributed microgrid," *IET Renewable Power Generation*, vol. 3, no. 2, pp. 109–119, 2009.

[15] A. Mohd, E. Ortjohann, D. Morton, and O. Omari, "Review of control techniques for inverters parallel operation," *Electric Power Systems Research*, vol. 80, no. 12, pp. 1477–1487, 2010.

[16] S. Khadem, M. Basu, and M. Conlon, "Parallel operation of inverters and active power filters in distributed generation system. a review," *Renewable and Sustainable Energy Reviews*, vol. 15, pp. 5155–5168, 2011.

[17] J. Guerrero, J. Matas, L. de Vicuna, M. Castilla, and J. Miret, "Wireless control strategy for parallel operation of distributed-generation inverters," *IEEE Transactions on Industrial Electronics*, vol. 53, no. 5, pp. 1461–1470, 2006.

[18] S. J. Chiang, C. Y. Yen, and K. T. Chang, "A multimodule parallelable series-connected pwm voltage regulator," *IEEE Transactions of Industrial Electronics*, vol. 48, no. 3, pp. 506–516, 2001.

[19] X. Zhang, H. Zhang, J. Guerrero, and X. Ma, "Reactive power compensation for parallel inverters without control interconnections in microgrid," *Conference of IEEE Industrial Electronics Society (IECON)*, pp. 922–925, 2008.

[20] K. Brabandere, B. Bolsens, J. Van den Keybus, A. Woyte, J. Driesen, and R. Belmans, "A voltage and frequency droop control method for parallel inverters," *IEEE Transactions on Power Electronics*, vol. 22, no. 4, pp. 1107–1115, 2004.

[21] Y. He, J.and Wei Li, "Analysis, design, and implementation of virtual impedance for power electronics interfaced distributed generation," *IEEE Transactions on Industry Applications*, vol. 47, no. 6, pp. 2525–2538, 2011.

[22] J. Matas, M. Castilla, L. de Vicuna, J. Miret, and J. Vasquez, "Virtual impedance loop for droop-controlled single-phase parallel inverters using a second-order general-integrator scheme," *IEEE Transactions on Power Electronics*, vol. 25, no. 12, pp. 2993–3002, 2010.

[23] W. Yao, M. Chen, J. Matas, J. Guerrero, and Z.-M. Qian, "Design and analysis of the droop control method for parallel inverters considering the impact of the complex impedance on the power sharing," *IEEE Transactions on Industrial Electronics*, vol. 58, no. 2, pp. 576–588, 2011.

[24] J. Kim, J. Guerrero, P. Rodriguez, R. Teodorescu, and K. Nam, "Mode adaptive droop control with virtual output impedances for an inverter-based flexible ac microgrid," *IEEE Transactions on Power Electronics*, vol. 26, no. 3, pp. 689–701, 2011.

[25] J. Kim, H. Choi, and B. Hyung Cho, "A novel droop method for converter parallel operation," *IEEE Transactions on Power Electronics*, vol. 17, no. 1, pp. 25–32, 2002.

[26] S. Yang, C. Zhang, X. Zhang, R. Cao, and W. Shen, "Study on the control strategy for parallel operation of inverters based on adaptive droop method," *IEEE Conference on Industrial Electronics and Applications.*, pp. 27–31, 2006.

[27] M. Chandorkar, D. Divan, and B. Banerjee, "Control of distributed ups systems," *IEEE Power Electronics Specialists Conference (PESC)*, vol. 1, pp. 197–204, 1994.

[28] J. Guerrero, J. Vasquez, J. Matas, L. de Vicuna, and M. Castilla, "Hierarchical control of droop controlled ac and dc microgrids. a general approach toward standardization," *IEEE Transactions on Industrial Electronics*, vol. 58, no. 1, pp. 158–172, 2011.

[29] M. Chandorkar, D. Divan, and R. Adapa, "Control of parallel connected inverters in standalone ac supply systems," *IEEE Transactions on Industry Application*, vol. 29, no. 1, pp. 136–143, 1993.

[30] A. Gil de Muro, J. Oyarzabal, and J. Nuñez, "Advanced architectures and control concepts for more microgrids," More microgrids project, Tech. Rep., 2010.

[31] S. Chiang and J. Chang, "Parallel operation of series-connected pwm voltage regulators without control interconnection," *IEEE Proceedings Electric Power Applications*, vol. 148, no. 2, pp. 141–147, 2001.